Check for updates

JGR Oceans

RESEARCH ARTICLE
10.1029/2020JC016614

Frontal Convergence and Vertical Velocity Measured by Drifters in the Alboran Sea

Daniel R. Tarry[1], Sebastian Essink[2], Ananda Pascual[1], Simón Ruiz[1], Pierre-Marie Poulain[3], Tamay Özgökmen[4], Luca R. Centurioni[5], J. Thomas Farrar[6], Andrey Shcherbina[2], Amala Mahadevan[6], and Eric D'Asaro[2]

[1]IMEDEA (CSIC-UIB), Esporles, Spain, [2]Applied Physics Laboratory, University of Washington, Seattle, WA, USA, [3]NATO-STO-CMRE, La Spezia, Italy, [4]Department of Ocean Sciences, University of Miami, Miami, FL, USA, [5]Scripps Institution of Oceanography, University of California-San Diego, La Jolla, CA, USA, [6]Department of Physical Oceanography, Woods Hole Oceanographic Institution, Woods Hole, MA, USA

Key Points:

- Kinematic properties were calculated from clusters of drifters at the surface (0.5–1 m) and subsurface (15 m)
- Vertical velocities estimates were obtained from drifter-calculated divergence
- A subduction event measured with a neutrally buoyant float was captured and is consistent with patterns of convergence measured from drifters

Correspondence to:
D. R. Tarry,
drtarry@imedea.uib-csic.es

Citation:
Tarry, D. R., Essink, S., Pascual, A., Ruiz, S., Poulain, P.-M., Özgökmen, T., et al. (2021). Frontal convergence and vertical velocity measured by drifters in the Alboran Sea. *Journal of Geophysical Research: Oceans*, *126*, e2020JC016614. https://doi.org/10.1029/2020JC016614

Received 26 AUG 2020
Accepted 14 MAR 2021

Abstract Horizontal and vertical motions associated with mesoscale (10–100 km) and submesoscale (1–10 km) features, such as fronts, meanders, eddies, and filaments, play a critical role in redistributing physical and biogeochemical properties in the ocean. This study makes use of a multiplatform data set of 82 drifters, a Lagrangian float, and profile timeseries of temperature and salinity, obtained in a ∼1-m/s semipermanent frontal jet in the Alboran Sea as part of CALYPSO (Coherent Lagrangian Pathways from the Surface Ocean to Interior). Drifters drogued at ∼1-m and 15-m depth capture the mesoscale and submesoscale circulation aligning along the perimeter of fronts due to horizontal shear. Clusters of drifters are used to estimate the kinematic properties, such as vorticity and divergence, of the flow by fitting a bivariate plane to the horizontal drifter velocities. Clusters with submesoscale length scales indicate normalized vorticity $\zeta/f > 1$ with Coriolis frequency f and normalized divergence of $\delta / f \sim \mathcal{O}(1)$ occurring in patches along the front, with error variance around 10%. By computing divergence from drifter clusters at two different depths, we estimate minimum vertical velocity of $\mathcal{O}(-100\ \text{m day}^{-1})$ in the upper 10 m of the water column. These results are at least twice as large as previous estimates of vertical velocity in the region. Location, magnitude, and timing of the convergence are consistent with behavior of a Lagrangian float subducting in the center of a drifter cluster. These results improve our understanding of frontal subduction and quantify convergence and vertical velocity using Lagrangian tools.

Plain Language Summary Vertical transport generated by mesoscale and submesoscale flows plays a key role in the exchange of physical and biogeochemical properties between the surface and the ocean interior. Using multiple simultaneous drifter observations, we compute spatial gradients of velocity to obtain estimates of the divergence field. Thanks to the fact that drifters were deployed at two different depths, we can observe the vertical dependence of divergence in the upper 15 m and estimate the associated vertical velocity. In this study, we estimate divergence and vertical velocity in a ∼1-m/s semipermanent frontal jet in the Alboran Sea by making use of a multiplatform data set including 82 drifters, a Lagrangian float, and along-shiptrack profile timeseries of temperature and salinity.

1. Introduction

The ocean's role in transporting heat and carbon from the surface to depth is crucial to regulate Earth's climate. Although deep convection and mixed-layer deepening dominate the vertical transport on seasonal timescales, vertical flows associated with mesoscale (10–100 km) and submesoscale (1–10 km) processes play a key role in the exchange of physical (temperature and salinity) and biogeochemical (nutrients, organic carbon, dissolved gasses, and pollutants) properties between the ocean surface and interior on shorter timescales. Previous studies that focused on vertical motion associated with mesoscale variability (characterized by a small Rossby number ($R_o = \zeta/f < 1$, where ζ is the relative and f the planetary vorticity) have reported vertical velocities of $\mathcal{O}(10\text{–}50\ \text{m day}^{-1})$ (Cotroneo et al., 2016; Estrada-Allis et al., 2019; Pallàs-Sanz et al., 2010; Pascual et al., 2004; Tintoré et al., 1991). At smaller scales, submesoscale flows are characterized by $R_o \sim 1$ providing a loss of balance of the mesoscale circulation and a cascade of energy to 3D dissipative turbulence. Submesoscale flows develop an ageostrophic secondary circulation at fronts that tends to restore geostrophic balance leading to surface convergences and vertical velocity. These flows

© 2021. American Geophysical Union. All Rights Reserved.

have a horizontal extent less than $\mathcal{O}$(10 km) and a life span of a few hours to days (Charney, 1971; McWilliams, 2016). Despite the fact that these are localized processes with short duration, recent studies have shown that the high intensity of the vertical flows accounts for a significantly larger vertical exchange than at the mesoscale (Ruiz et al., 2019; Siegelman et al., 2020; Yu et al., 2019).

However, vertical velocities represent a challenge to measure or estimate due to their small horizontal scales and magnitude which is typically 3–4 orders of magnitude smaller than the mesoscale horizontal velocities. Traditional Eulerian observing systems, such as shipboard acoustic Doppler current profilers (ADCPs), lack the accuracy and resolution to capture the small-scale signal of these vertical velocity fields. Only recently, with the development of new Lagrangian tools (D'Asaro, 2003; Novelli et al., 2017), it has become possible to observe small-scale intense convergences. For example, D'Asaro et al. (2018) measured vertical velocities of $\mathcal{O}$(1,700 m day^{-1}) in the upper 30 m of the water column with a Lagrangian float designed to follow the full 3D Lagrangian flow. Likewise, an increase in model resolution enables us to study these processes numerically and to understand their importance for the vertical exchange of properties (Freilich & Mahadevan, 2019; Mahadevan & Tandon, 2006).

The Alboran Sea, located in the Western Mediterranean, provides a favorable scenario to measure vertical velocities. Where the inflowing Atlantic waters from the Gibraltar Strait encounter the denser Mediterranean waters, sharp density fronts are created (Tintoré et al., 1988) that are readily identified from satellite imagery and can be observed year-round. These density fronts become unstable and generate an intense ageostrophic secondary circulation associated with surface convergence and strong vertical velocity (Lévy et al., 2001; Mahadevan & Archer, 2000; Mahadevan et al., 2016; McWilliams, 2016; McWilliams et al., 2019). Evidence for these vertical motions in the Alboran Basin has previously been observed by other authors (Allen et al., 2001; Flexas et al., 2006; Oguz et al., 2014; Pascual et al., 2017; Tintoré et al., 1991) who found strong signals of subduction in physical and biogeochemical properties (Ruiz et al., 2009, 2019).

Here, we use a large drifter data set in the Alboran Sea as part of the ONR Departmental Research Initiative, "CALYPSO" (Coherent Lagrangian Pathways from the Surface Ocean to Interior) (https://calypsodri.whoi.edu/), whose goal is to better understand the three-dimensional pathways of Lagrangian particles in the ocean. Vertical advection of particles by submesoscale currents can significantly increase the vertical flux of nutrients or organic matter (e.g., Mahadevan & Tandon, 2006; Omand et al., 2015). Therefore, understanding submesoscale features that give rise to vertical motion is of crucial concern. Several studies in the Mediterranean Sea have used drifters to map the currents and compute dispersion (Alpers et al., 2013; Poulain et al., 2013; Sotillo et al., 2016), however, this study is the first with dense drifter deployments to focus on the calculation of the kinematic properties of the flow in this region, such as the vertical component of relative vorticity $\zeta = v_x - u_y$ and horizontal divergence $\delta = u_x + v_y$. The large numbers of colocated drifter clusters available in this experiment is used to reduce the uncertainty in the velocity gradient calculation. Paired with significantly improved GPS accuracy (5–10 m) and high temporal resolution (5 min), previous authors (Berta et al., 2016; LaCasce, 2008; Ohlmann et al., 2017) were able to retrieve estimates of vertical vorticity, lateral strain rate, and horizontal divergence at submesoscales in other regions.

In this study, we estimate the kinematic properties of the flow from a set of surface and near-surface drifters deployed in a 2-km-wide front in the Eastern Alboran Gyre. Thanks to an optimized deployment scheme that spans a wide range of scales (Figure 1b), it is possible to analyze the dynamics in the mesoscale and submesoscale range. The estimation of kinematic properties at two different depths allows us not only to observe the horizontal distribution but also get an idea of the vertical dependence in the upper 15 m. The divergence estimated from drifters during a strong subduction event is compared to the trajectory of a 3D Lagrangian float which is able to measure vertical velocity from two methods: the high-frequency upward-looking ADCP and the time derivative of the pressure measurement.

This study is structured as follows. First, in Section 2, brief introductions are given to the Alboran Sea as well as the drifter and float deployments. In Section 3, we detail the methodology followed to estimate kinematic properties and vertical velocities from clusters of drifters. In Sections 4 and 5, we present and discuss our results found at a subducting submesoscale front. We conclude our analyses in Section 6.

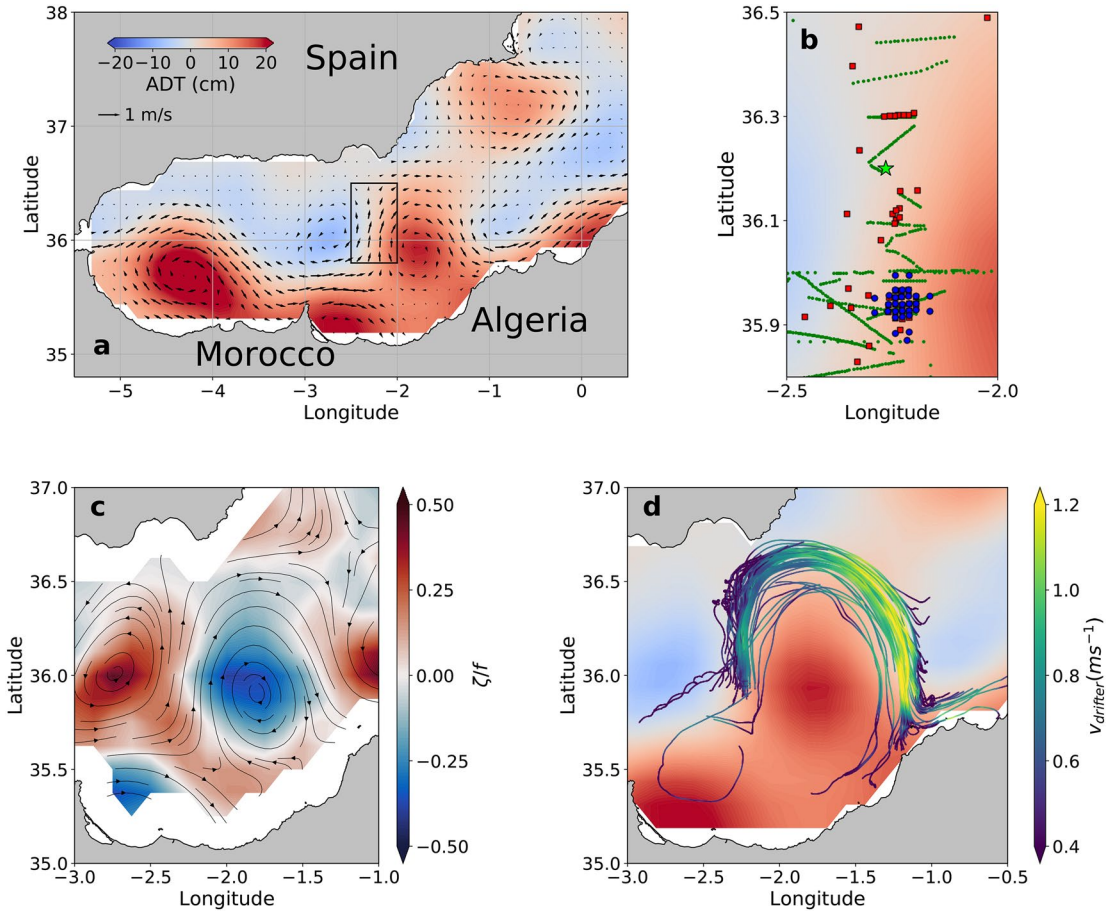

Figure 1. (a) Absolute Dynamic Topography (ADT) (CMEMS, Ducet et al., 2000) for May 31, 2018 in the Alboran Sea. The black arrows represent the geostrophic circulation. The black box indicates the region shown in panel (b) where the main measurements were taken (May 31 to June 2, 2018). (b) Deployment locations for surface drifters (red squares), near-surface drifters (blue dots), and the Lagrangian Float (limegreen star). UCTD sampling is shown with green dots. (c) Vorticity field derived from the ADT in (a). Arrows indicate the mean flow. (d) Trajectories of drifters deployed in (b) from May 31, 2018 to June 4, 2018 with drifter velocity in color. UCTD, Underway-CTD.

2. Observations

2.1. Region of Study: Alboran Sea

The Alboran Sea is the westernmost basin of the Mediterranean Sea, a semiclosed sea connected to the Atlantic Ocean through the Strait of Gibraltar. The imbalance caused by greater evaporation than precipitation and river runoff is compensated by a strong inflow of Atlantic waters into the basin. The strong barotropic and baroclinic flow instabilities present in the Alboran Sea cause the inflowing waters to form a sequence of gyres of high intensity (Allen et al., 2008). Except for certain periods of the year, the circulation in the Alboran basin is dominated by a quasi-permanent Western Alboran Gyre and a more variable Eastern Alboran gyre (EAG) (Renault et al., 2012). As these waters leave the Alboran Sea, they flow eastward at the surface along the Algerian slope creating the Algerian Current (Figure 1a).

During spring and summer, as a consequence of positive air-sea heat fluxes, the region is thermally stratified, manifesting in shallow mixed-layer depths (MLD) between 5 and 15 m (Houpert et al., 2015; Mason et al., 2019). Due to strong shallow stratification, the mixed-layer dynamical processes might be disconnected from the layers below the MLD and vertical exchange between surface and interior is largely inhibited. During fall and winter, however, stratification weakens and mixed-layer processes are able to penetrate deeper, potentially reaching below the seasonal thermocline. In addition to seasonal variation in heat fluxes, lagoonal dynamics of the Mediterranean Sea generate larger influx of Atlantic water in the summer when the pressure gradient is largest.

2.2. Data

The 2018 CALYPSO experiment took place in the eastern Alboran Sea between May 27 and June 2, 2018 on board of the *NRV Alliance* and *RV SOCIB*. Multiple platforms were used in the cruise (Mahadevan et al., 2020). In this study, we make use of the drifter, Underway-CTD (UCTD), and a neutrally buoyant Lagrangian float data sets.

2.2.1. Drifters

To compare kinematic properties at different depths, a total of 82 drifters drogued at three different depths were deployed. To resolve the kinematic properties, we divided the data set into surface (0.6 and 1 m) and near-surface (15 m) drifters. The surface drifters include the Consortium for Advanced Research on Transport of Hydrocarbon in the Environment (CARTHE) and the Coastal Ocean Dynamics Experiment (CODE) drifter. The CARTHE drifters consist of a buoy attached to a drogue that extends 60 cm below the surface, designed to be ecofriendly (85% biodegradable), compact, and low cost (Novelli et al., 2017) and, therefore, optimal for large array deployments (D'Asaro et al., 2018; Haza et al., 2016). During the experiment, a total of 35 CARTHE drifters were deployed and transmitted their GPS position every 5 min. The CODE drifters follow the top 1-m average current (Davis, 1985; Poulain & Gerin, 2019). Fourteen CODE drifters transmitted their position every 10 min. Both sets of surface drifters experience a veering from the actual current due to wind slippage. Previous work established this wind-current to be about 10% of the wind speed experienced by the drifter (Mauri & Poulain, 2004; Niiler et al., 1995; Poulain et al., 2009; Rio & Hernandez, 2003). The Surface Velocity Program (SVP) drifters consist of a surface buoy attached to a drogue centered at 15 m depth (Sybrandy & Niiler, 1991). During the experiment, a total of 33 SVP drifters were deployed which transmitted their GPS position every 5 min. On May 31, an array of 51 drifters (9 CARTHE, 13 CODE, and 29 SVP) was deployed in a hexagonal shape on the upstream region of the EAG. This deployment shape, with a maximum cross-array length of 12 km, was designed to resolve the submesoscale and mesoscale kinematic properties of the gyre (Figure 1b). The data set, including all three drifter types, was processed to remove spikes in velocity and acceleration, interpolated to 5 min, and filtered with a 1-h hamming window.

2.2.2. Lagrangian Float

Vertical velocity was measured by a neutrally buoyant Lagrangian float (D'Asaro, 2003) designed to follow the three-dimensional motion of water parcels by combining a density close to that of the water and a high drag. Figure 2a shows data from the first few hours of the float deployment. The float was deployed in the early morning of June 1 within a filament of dense water on the dense side of the front (Yellow dot 1, Figure 2) and within the drifter array. It then surfaced, took a GPS fix, dove to 40 m and then near yearday 152.15, began a Lagrangian drift starting at the surface. The float remained at the surface until at about yearday 152.23 when it left the surface, descended to about 10 m and then returned to the surface about 2,900 s later. A major goal of this paper is to describe this event.

During the Lagrangian drift, the float continuously adjusted its density to match that measured by the onboard CTDs. Depth is plotted in Figure 2a and density from the top and bottom CTDs in Figure 2b. The density measured on the float is compared to that from the TSG (Figure 2b, magenta line) and the shallowest good data point from each UCTD profile (blue dots). Differences of up to 0.02 kg m^{-3} between the UCTD and ship intake values are evident perhaps due to stratification between the intake at a few meters depth and the first good UCTD data at 6-m depth.

The only exact float position is obtained from the GPS fix near yellow circle one in Figure 2. Estimated float positions over the next 20,000 s (5.5 h) are computed from the average position of four surface drifters that were within about 1 km of the float at launch. Tracks of the ship, the four drifters and the estimated float positions are shown in Figure 2c.

The float measures vertical velocity in two complementary ways. First, to the extent that the float moves with the water, the vertical velocity of the float is the vertical velocity of the water. Second, the float carries an upward-looking, 1,000-kHz five-beam Nortek Signature ADCP. Vertical velocity of the water relative to the float is measured both by the fifth beam, which looks directly along the float, and from the four-slant

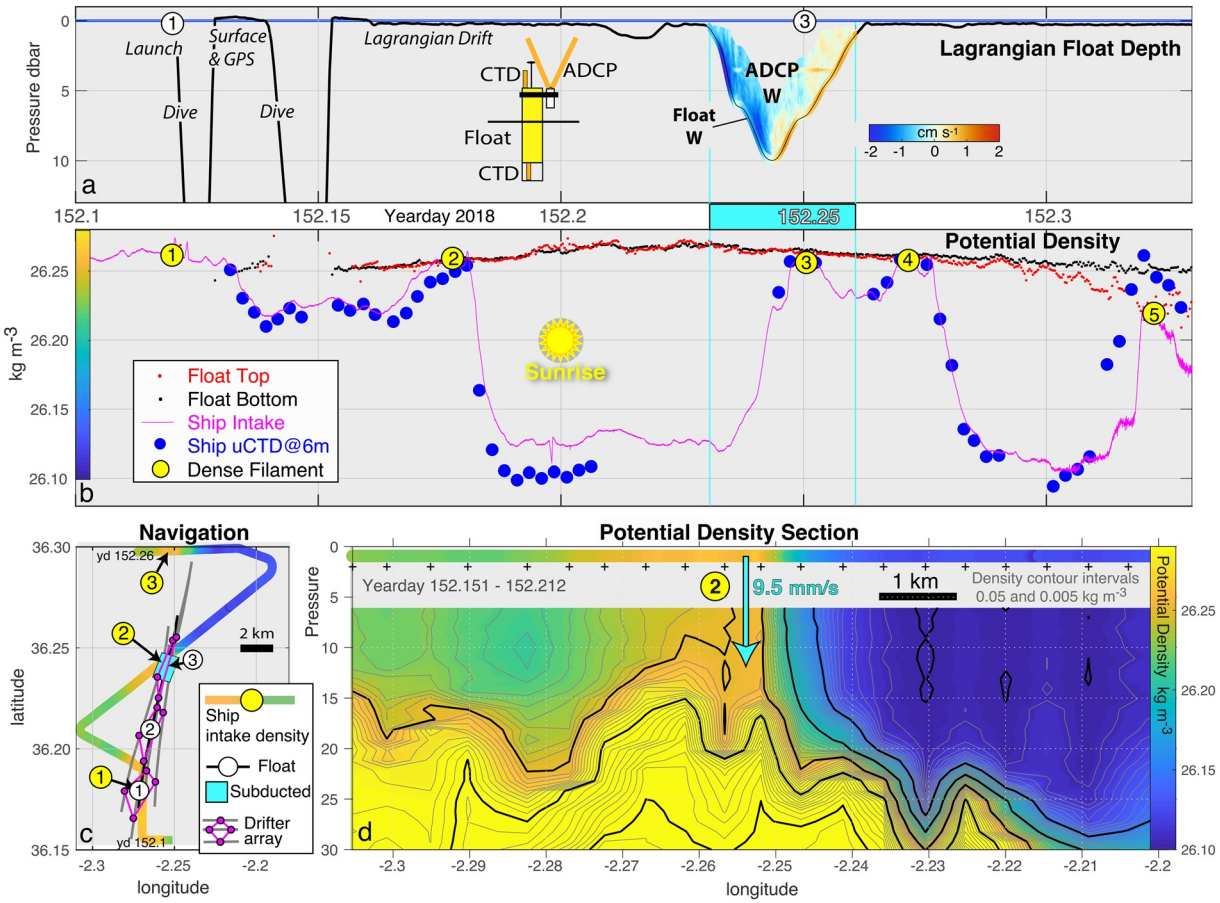

Figure 2. Lagrangian Float deployment. (a) Depth of the CTD intake at the top of the float as a function of time for the first few hours (yeardays 152.1–152.33) of the deployment (black line). A cartoon of the float is shown. After deployment, the float followed its program: first diving, reaching 27 m, then surfacing to get a GPS fix, and then diving again, reaching 40 m before beginning a Lagrangian drift starting at the surface. From about yearday 152.23 to 152.26 (cyan/blue shading on time axis), the float subducts to ≈10 m before returning to the surface. During this event, the measured vertical velocity is shown in color, with the float velocity plotted beneath and the ADCP velocity plotted above the black line. (b) Potential density timeseries, as measured by the CTD at the top of the float (red dots), and at the bottom of the float (black dots), by the ship intake (magenta curve) and by the UCTD at its shallowest depth (≈6 m). (c) Platform tracks: shiptrack (colored by intake density and annotated with yellow circles) and float track (black annotated with white circles). The float track is estimated from the average of the four closest drifters (gray with small magenta circles connected by magenta lines). For clarity, data are only shown through yearday 152.26 as six overlapping repeat sections were then made along 36.30°N. (d) Potential density section extending northeast from about 36.1°N to 36.2 9°N. Top data are from ship intake; bottom data from UCTD. Small " + " shows the location of the UCTD profiles. Black bar shows a 1 km cross-frontal distance. Cyan/blue rectangles between (a) and (b) and in (c) show the duration of the float subduction. Cyan/blue arrow shows the vertical excursion of a water parcel during this event starting near the surface as measured by the Lagrangian float. In all panels, yellow numbered circles mark times of local maximum surface density measured by the ship, e.g., a crossing of the dense filament. White and magenta circles in (c) mark these times along the float and drifter trajectories, respectively. Circle "1" correspond to the approximate float launch time; circle "3" to the approximate time of maximum float subduction. The time of sunrise is marked by the sun image. ADCP, acoustic Doppler current profilers; UCTD, Underway-CTD.

beams that look at 25° from the float axis in a Janus configuration. For each beam, velocity measurements are made in both a broadband (BB) mode, with a vertical resolution of 1 m and a single ping vertical velocity accuracy of about 0.01 m s^{-1} and a high-resolution (HR) mode with 0.025 m bins and single ping vertical velocity accuracy of about 0.001 m s^{-1} (Shcherbina et al., 2018), but a range of only 4 m. Long ranges are not necessary, so the four-beam HR data, rotated to East, North and Up based on the ADCP's magnetic and tilt sensors, was used here. The absolute vertical velocity is obtained by adding the pressure-derived vertical velocity of the float to the relative ADCP measurements. Results using the BB data, either the four-beam or the fifth beam, are similar, but with less resolution and accuracy. The vertical velocity from both the float pressure sensor and from the ADCP are shown in the color swath in the center of Figure 2a during the float subduction event.

2.2.3. Underway-CTD

Repeated timeseries profiles of temperature (T) and salinity (S) were collected using the Underway-CTD (UCTD). The UCTD probe, which measures conductivity, temperature, and pressure (Rudnick & Klinke, 2007), was deployed from the stern of the *NRV Alliance*, allowing it to free fall for 90 s and measure T and S in the upper 200–250 m. The UCTD was calibrated against the ship's Seabird 9/11 CTD at the beginning and end of the cruise to an estimated accuracy of 0.006 psu and 0.005 °C (Dever et al., 2019). The time needed for one profile was about 5 min, which at a steady ship speed of 6 kt corresponds to a horizontal resolution of about 1 km. The vertical sampling rate was 16 Hz, which was filtered and binned to a 0.5-m vertical grid (see Dever et al., 2019). After the drifter deployment, the ship repeatedly traversed back and forth across the path of the drifters to produce UCTD sections for a high-resolution hydrographic context (Figure 1b). An example is shown in Figure 4.

2.2.4. Altimetry Maps

We use daily delayed-time Absolute Dynamic Topography (ADT) and surface geostrophic current maps. Altimeter satellite gridded ADT are computed with respect to a 20 2012 mean. The ADT is estimated by Optimal Interpolation, merging the measurement from the different altimeter missions available into a regular 1/8° grid. This product is processed by the DUACS multimission altimeter data processing system. It processes data from all altimeter missions: Jason-3, Sentinel-3A, HY-2A, Saral/AltiKa, Cryosat-2, Jason-2, Jason-1, T/P, ENVISAT, GFO, ERS1/2. The geostrophic currents are derived from ADT.

2.2.5. Ship Intake Thermosalinograph

The ship thermosalinograph (TSG) measured temperature and salinity of water drawn into the ship from a few meters depth. To intercalibrate, the measured TSG salinity is increased by 0.02 psu and its temperature reduced by 0.55 °C to best match the shallowest points in the UCTD profiles from the entire cruise.

3. Estimation of Kinematic Properties and Vertical Velocity

Different techniques have been proposed to estimate the velocity gradients of a flow field from observational drifter data (Kawai, 1985; Molinari & Kirwan, 1975; Okubo & Ebbesmeyer, 1976; Saucier, 1955).In this work, we will focus on the linear Least Squares (LS) method used by Molinari and Kirwan (1975) to obtain the velocity gradients from a cluster of drifters. The advantage of this approach over other methods is that there is no difficulty in extending the calculation to a larger number of drifters per cluster and it has previously been applied to Lagrangian data (Berta et al., 2020; Niller et al., 1989; Ohlmann et al., 2017; Paduan & Niiler, 1990; Swenson et al., 1992). Furthermore, the statistical confidence in the results increases with the number of drifters. In other words, the velocity gradient calculation is less sensitive to a single drifters' position uncertainty.

$$\begin{aligned} u_i &= \overline{u} + \frac{\partial u}{\partial x}(x_i - \overline{x}) + \frac{\partial u}{\partial y}(y_i - \overline{y}) + \mathcal{O}\left((x_i - \overline{x})^2\right), \\ v_i &= \overline{v} + \frac{\partial v}{\partial x}(x_i - \overline{x}) + \frac{\partial v}{\partial y}(y_i - \overline{y}) + \mathcal{O}\left((y_i - \overline{y})^2\right). \end{aligned} \tag{1}$$

Since this is a linear method, the expansion is truncated at first order. The remaining higher orders include measurement, process errors, and higher order components of the velocity field. (Molinari & Kirwan, 1975). For each of the drifters, the position (x_i, y_i) and velocity (u_i, v_i) are known from the GPS data. The three unknowns in each of Equation 1 are the velocity of the center of mass, and the two components of the velocity gradient. Thus, three drifters are needed for this system to be solvable exactly. Increasing the number of drifters per cluster, reduces the error of the fit in a least square sense. The details to solve this system of equations to obtain the velocity gradients can be found in Molinari and Kirwan (1975).

The number of drifters, the length scale L, and the aspect ratio are important for the accuracy in the velocity gradient estimate. The length scale L of the cluster is important since the LS method was devised for small separation distances and/or a linear velocity field. A further detailed view of this can be gained from the

Taylor expansion in Equation 1 where small-scale variability of $\mathcal{O}(\Delta x^2) = \mathcal{O}(\Delta y^2)$ is assumed small and truncated. We define the length scale of a cluster as the root mean squared distance of all pairs of drifters. The method is accurate as long as the cluster is not larger than the scale to be resolved. The aspect ratio α defines the regularity of a cluster. Mathematically, this is represented as the ratio between the minor and major eigenvalues of the position covariance matrix, $\alpha = \lambda_{\min}/\lambda_{\max}$ (Choi et al., 2017). A regular cluster will have an aspect ratio of one, while an elongated cluster will have an aspect ratio close to zero. Clusters with aspect ratio close to zero will produce velocity gradient estimates with a low correlation with respect to the actual velocity field. In other words, the cluster is no longer measuring the 2D velocity gradients properly due to the irregular shape. Therefore, those clusters with an aspect ratio smaller than 0.1 will be excluded.

The accuracy of the method due to systematic GPS error can be quantified following the work by Spydell et al. (2019). In particular, the vorticity error variance is given by

$$\sigma_\zeta^2 = \frac{1}{N}\frac{\sigma_u^2}{l_a^2}\left(1 + \frac{l_a^2}{l_b^2}\right)\left(1 - \rho_{u_1u_2}\right), \tag{2}$$

where N is the number of drifters per cluster, l_a and l_b are the lengths of minor and major axis of the drifter cluster, σ_u is the velocity error due to the GPS error and $\rho_{u_1u_2}$ is the velocity error correlation. We can assume $\rho_{u_1u_2} = 0$ as it tends to zero for spatial scales larger than $\mathcal{O}(10^2$ m) and represents an upper bound for the drifter observations presented here (Spydell et al., 2019).

We obtain cluster-averaged kinematic properties from the computed velocity gradients for all available clusters. The total number of clusters is given by all combinations of six drifters without repetitions, given by the binomial coefficient, $\binom{K}{6}$, where K is the total number of drifters. A total of nearly 14 million combinations are obtained for the surface data set (49 drifters) and 1 million combinations for the near-surface data set (33 drifters). However, the actual number of results is less as many clusters are filtered out following the length scale and aspect ratio criteria discussed above.

We obtain cluster-averaged kinematic properties from the computed velocity gradients for all available clusters formed by six drifters. Molinari and Kirwan (1975) showed that the standard deviation of the kinematic properties decreases with number of drifters per cluster. Furthermore, Equation 2 in Spydell et al. (2019) shows that the vorticity error due to GPS uncertainty is inversely proportional to the number of drifters. Therefore, we expect to obtain more precise results than when using three drifters per cluster. Larger numbers of drifters could raise two difficulties. First, we are interested in clusters with mesoscale and submesoscale length scales. However, the more drifters are used per cluster, the larger the cluster scale will be on average. Second, the total number of clusters is given by all combinations of six drifters without repetitions, given by the binomial coefficient $\binom{K}{N}$, where K is the total number of drifters and N is the number of drifters per cluster. With six drifters per cluster, a total of nearly 14 million combinations are obtained for the surface data set (49 drifters) and 1 million combinations for the near-surface data set (33 drifters). Higher numbers of drifters per clusters will increase the total number of clusters to a great extent, rapidly increasing the computational cost needed to perform the calculation on all available clusters. However, the true number of clusters used is less than the total number of possible combinations because many clusters are filtered out following the length scale and aspect-ratio criteria discussed above.

The vertical velocity difference between two depth levels h_1 and h_2 can be estimated by integrating the divergence vertical profile (Equation 3):

$$\Delta w = w(z = h_2) - w(z = h_1) = -\int_{z=h_1}^{z=h_2} \left(u_x + v_y\right) dz. \tag{3}$$

Since we compute divergence from drifter clusters at two depths, we assume a linear profile. If we consider $h_1 = 0$ m, we obtain an estimate of the vertical velocity at $z = h_2$ (Equation 4, since vertical velocity at surface is assumed to be zero (i.e., $w(z = h_1) = 0$)).

$$w(z = h_2) = -\int_{z=0}^{z=h_2} \left(u_x + v_y\right) dz. \quad (4)$$

4. Results

4.1. Float Subduction

After deploying the float (yellow circle "1") the ship crossed the front twice (Figure 2c) moving ahead of a dense drifter cluster and the float to avoid impacts. Repeated sections were then conducted along 36.3°N to avoid ship traffic north of there. The float and four surrounding drifters moved north more slowly. The float subducted at about 36.24°N (roughly at white circle "3") with the cyan/blue rectangles (Figures 2a–2c) marking the time during which the float was subsurface. The ship passes through this point (yellow circle "2") about 63:00 s (1.74 h) before the float subduction. The associated section (Figure 2d) will be used to interpret the float data.

The combination of UCTD sections and underway density along multiple frontal crossings shows the density structure in the subduction region. At the surface, the front separates lighter, colder, fresher Atlantic water to the east and heavier, saltier, warmer Mediterranean water to the west, with the densest water appearing in a 1–2 km wide filament just west of the front. The float was intentionally deployed in this filament. Timeseries of density observed by the ship and float (Figure 2b) show the float density remaining at 26.26 ± 0.01 kg m^{-3} with the ship's thermosalinograph and UCTD reaching within ± 0.05 kg m^{-3} of the float value at the maximum density of each frontal crossing. Each of these times is marked by a yellow circle in Figure 2. The vertical structure of the front is shown in Figure 2b. Isopycnals upwell to the surface at the front to form the dense filament, with water-mass properties from just below the mixed layer to the west. The mixed layer is about 15-m deep on the denser side to the west, shallowing to less than 6 m at the front and then deepening to almost 20 m in the lighter side to the east. Similar structures are measured in the other sections. Despite considerable variability, the dense filament is a persistent structure of this front through the early morning of June 1 (yearday 152). However, by midmorning the surface layer begins to rapidly warm and stratify due to solar heating, as is evident near crossing "5," capping the dense filament and likely inhibiting vertical exchange from the surface.

After deployment and two short profiles (Figure 2a), the float moves along the front within the dense filament surrounded by the four tracking drifters. The drifters converge and, 94:00 s (2.4 h) after launch, the float rapidly sinks to about 10 m and then returns to the surface. It moves downward with an average speed of 8.6 mm s^{-1} (740 m day^{-1}) (blue on the color scale) and returns up with an average speed of 6.2 mm s^{-1} (540 m day^{-1}) (orange on the color scale). ADCP measurements 0.5–1.5 m above the ADCP measure average downward speeds 8.2–10.9 mm s^{-1} (blue on the color scale) and average upward speeds 1.8–0.5 mm s^{-1} (light yellow on the color scale). This implies that the float is slightly buoyant, with an average upward velocity relative to the water of about 1 mm s^{-1} on the downward leg and 5 mm s^{-1} on the upward leg. These correspond to a downward displacement of the water relative to the float of less than 1 m on the downward leg and about 7 m on the upward leg. Thus, although the float returns to the surface, this motion is probably due to its buoyancy and does not reflect the motion of the water. The water probably descends somewhat deeper than the bottom CTD of the float at 11.5 m, perhaps to the base of the mixed layer at 12–15 m. The water probably moves upward only a few meters during the float's ascent. Thus, the float measurements imply that water is subducted from within a few meters of the surface to 12–15 m at a mean downward speed of 9.5 ± 1 mm s^{-1} and probably remains below the surface while the float returns to the surface. This is shown by the cyan/blue arrow in Figure 2d. The water's motion after this time was not measured.

4.2. Mesoscale Kinematic Properties

We divide up our analysis of kinematic properties based on length scale: first, we present the mesoscale results; then, we present the submesoscale results in the following subsection together with a comparison to simultaneous Lagrangian float and underway-CTD observations.

The length scales chosen for the mesoscale analysis of the kinematic properties in the EAG are $10 < L < 40$ km. Since the radius of the gyre in which the drifters are deployed is about 50 km, we expect the velocity gradients calculated from clusters of length scales lower than 40 km to keep correlation with the mesoscale flow field. Although the smaller scales ($L < 10$ km) are filtered out by large clusters, we expect small-scale variability to be aliased. Hourly kinematic properties are computed with clusters that meet the length scale and aspect-ratio requirements. The calculation starting on 05-31 14:00 h is terminated after 72 h when most of the drifters left the gyre and entered the Algerian Current following the African north coast. Binned maps of normalized divergence δ/f and vertical vorticity ζ/f are shown in Figure 3. The plotted values are given by the median of all data points contained in each bin.

Just some hours after the drifter deployment, at $t = 7$ h, surface clusters show two regions of opposite sign of divergence at the beginning of the drift (western side of the gyre), with negative divergence (convergence) at the outside edge and positive divergence in the interior. The absolute median divergence value at both sides is around $0.25f$. Near-surface clusters are located in the inner part showing divergence around $0.2f$. At $t = 25$ h, the divergence signal intensifies both at surface and subsurface reaching values of $0.4f$. Finally, on the eastern side of the gyre, at $t = 70$ h, the surface clusters show a large region of convergence with minimum values of $-0.4f$. At this time, near-surface drifters have already passed through this point showing a much weaker convergence ($-0.1f$). The divergence at the eastern edge is likely due to the eastward advection of drifters by the Algerian Current. Overall, the convergence is only present at the surface and appears not to reach down to 15-m depth.

At the beginning of the drift the clusters generate positive values of relative vorticity of about $0.2f$. Once the drifters pass the 36.4°N latitude, vorticity starts to become more negative with $-0.5f$. As they reach the easternmost part of the gyre, positive values dominate again.

4.3. Submesoscale Dynamics

We now focus on the first few hours of deployment, when the initial drifter array has not spread apart. It is in this period of time when we have the largest amount of clusters in the submesoscale length scale range. As drifters advance through the gyre, they spread apart, clusters get elongated and grow in size. Since we want our results focused on the submesoscale, we not only select those clusters below the 10-km length scale L (the Rossby radius in the region is around 14 km (Escudier et al., 2016), and we therefore expect that the submesocale kinematic properties should be captured) but we also decrease the time step of the LS method to 10 min. The increase in both space and time resolution should allow us to capture the high variability of the kinematic properties.

Binned maps of horizontal divergence at surface at different timestamps are shown in Figure 4). As in Figure 3, each bin is represented by the median of the results contained on it. The results from the near-surface clusters are not shown as they did not show variability from a uniform divergence of $\sim 0.5f$. The same is true for the vorticity results, for which positive values $\sim 1f$ were obtained consistently throughout the analysis. However, the surface divergence results show a high space-time variability. This variability is particularly visible between timestamps t_2 (05-31 10:40 h; Figure 4b) and t_{43} (06-01 00:30 h; Figure 4c). In the vicinity of the frontal region at 36.15 N, in barely 2 h the divergence signal turns from positive ($0.3f$) to negative ($-0.6f$). The variability is not only temporal but also spatial. The intense signal of convergence is just 4–5 km wide, while the rest of the clusters still indicate weak divergence. This is also apparent in timestamp t_4 (06-01 03:30 h; Figure 4d) which also shows the high spatial variability of the divergence field, where clusters below 36.2°N show divergence up to $0.4f$ while the northern clusters measure week convergence ($-0.2f$).

We examine the drifter-derived submesoscale kinematic properties in the vicinity of the subduction location of the Lagrangian float. This will test the capacity of drifters to characterize a subduction event, occurring at high intensity, short duration, and small scale. Since the position of the float is unknown once it is subsurface, it is assumed that the float follows the same patch of water as the four closest drifters. The choice of threshold radius is a trade-off between having enough drifters to apply the LS method and keeping the clusters length scale in the submesoscale range. With these criteria, all drifters inside a 6-km radius were selected, which sum up to 18 surface drifters (18,564 clusters) and 10 near-surface drifters (210 clusters). Although smaller threshold radius would decrease the cluster length scale, it would limit the number

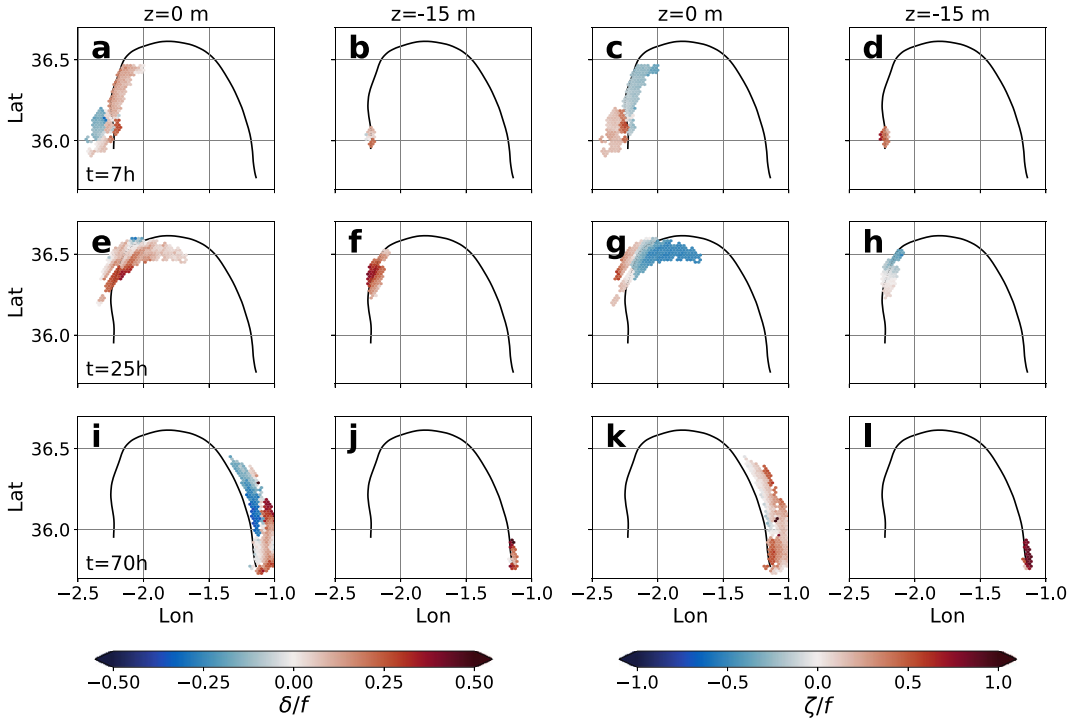

Figure 3. Normalized divergence δ/f (a, b, e, f, i, and j) and vertical vorticity ζ/f (c, d, g, h, k, and l) obtained from drifters while traveling along the Eastern Alboran Gyre. The first and third column correspond to values at surface while the second and fourth column show values at 15-m depth. Top row is at 7 h, the middle row 25 h, and the bottom row is 70 h after the start of the analysis. Each bin represents the median value of the clusters that contains at least 10 data points. The black line is a representative trajectory of the drifters that followed the mean flow along the Eastern Alboran Gyre.

of drifters for applying the LS method. In this case, considering a radius of 5 km, there were only seven near-surface drifters available, lowering considerably the statistical stability of the results.

The probability density functions (PDF) of the normalized horizontal divergence calculated from the surface and near-surface drifters around the float for different times are shown in Figures 5b–5g. Figure 6 shows the spatial distribution of the surface divergence (and vorticity) at times t_1 and t_3 from Figure 5 together with a UCTD section near the subduction location. Before the float subducts at t_1 (06-01 05:20 h), the surface clusters show convergence with mean values of $-1f$ and extreme values near the front of $-2f$ (Figures 5b and 6b). Unlike this strong convergence at the surface, the near-surface clusters at 15 m show smaller divergence around $0.5f$ (Figure 5e). As the float reaches its maximum depth at t_2 (06-01 5:50 h), there is an important change in the PDF of surface divergence (Figure 5c). The divergence follows a bimodal distribution of near-zero mean but one peak located at $-0.8f$ and the other at $0.3f$. A large number of clusters showed increasing divergence by $1f$ within just 30 min. Meanwhile at 15 m, the divergence only slightly increased by $0.1f$. Once the float is back at the surface (t_3, 06-01 6:30 h), the divergence at the surface follows a negatively skewed, single-peak distribution. The divergence values range from $-1.5f$ to $0.5f$. Clusters with these divergence values are mostly located north of the UCTD track (Figure 6c).

We focus on the vertical velocity calculation from drifter-computed divergence. As we explained in the methods section, we need a vertical profile of divergence to integrate Equation 4. To be able to compare with the vertical velocity measured by the float later, we focus on the drifter-computed divergence at t_1 in Figure 5, just before the float subducts. If we use the median values of the PDFs in Figure 5 ($-1f$ at the surface and $0.35f$ at 15 m), we obtain a vertical velocity at 10-m depth of -45 m day^{-1}. We can estimate the vertical velocity from clusters measuring the strongest convergence. To minimize the possible noise due to errors (specially at the surface), we select the 5% percentile of the PDFs ($-2f$ at the surface and $-0.05f$ at 15 m). With these divergence values we obtain a vertical velocity at 10-m depth of -100 m day^{-1}.

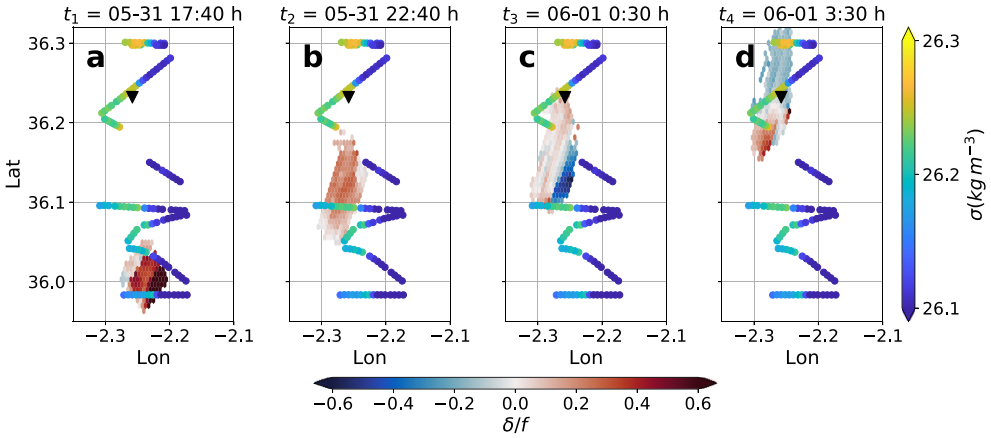

Figure 4. Normalized divergence δ/f calculated with a 10-min timestep for surface clusters of length scale $L < 10$ km. Colored points representing the potential density anomaly are plotted from UCTD data at the surface ($z = -2$ m). The downward triangle shows the location of the float subduction. Panels (a) to (d) correspond to different timestamps: (a) May 31, 2018 17:40 h, (b) May 31, 2018 22:40 h, (c) June 1, 2018 00:30 h, and (d) June 1, 2018 03:30 h.

UCTD data complements float and drifter data, providing information of the temporal and spatial variability of the front. The time evolution of the potential density in a repeated UCTD section (track located at 36.3°N in Figure 6) is shown in Figure 7. The front location is determined by the maximum horizontal gradient of surface density. In the first section, the front is located at 2.23°W and remains almost constant for the first three timesteps (2 h). Just one hour later (Figure 7d), the isopycnals start to slant, continually decreasing the intensity of the front over the following sections. By the last section, the state of the front has largely changed in a period of just 3 h. The relaxation of the front, mainly by tilted isopycnals located at the surface, is shown at Figures 7g and 7h. Before the relaxation of the front, at about 5 m, there is a maximum horizontal gradient of 0.2 kg m^{-3} over 2 km. Once the front weakens, the last section shows a gradient of 0.1 kg m^{-3} over 4 km. Meanwhile at 10 m, the intensity of the gradient remains constant at 0.2 kg m^{-3} over 3 km, although shifted to the west.

5. Discussion

5.1. Kinematic Properties Findings

In the mesoscale range, the divergence on the west side of the EAG implies upward vertical velocity. The convergence on the east side of the EAG implies downward vertical velocity. These results match with the quasi-geostrophic vertical velocities expected from such a meander. Previous studies have reported positive vertical velocities where anticyclonic vorticity dominates and negative vertical velocities where cyclonic vorticity dominates (Cotroneo et al., 2016; Gomis et al., 2001; Pascual et al., 2004; Tintoré et al., 1991). The large-scale pattern is consistent with the vorticity field derived from the absolute dynamic topography (Figure 1c) (Ducet et al., 2000; Traon et al., 1998). The vorticity field is mostly negative due to the circulation of the gyre and changes to positive when clusters run into the Algerian Current.

At the submesoscale, our results are consistent with previous drifter studies that focused on the kinematic properties at this scale. Using triplets of drifters in the Golf of Mexico (Berta et al., 2016), computed divergence and lateral strain rate using Saucier's method. Although their computation is based on a limited number of triplets, values of $\mathcal{O}(f)$ were found (Ohlmann et al., 2017). used the LS in the Gulf of Mexico but on triplets of drifters. They found strong convergence and positive vorticity of multiple times f regions of submesoscale fronts. In eddies, weaker magnitudes and smaller skewness of the probability density functions were found.

From a dynamical point of view, the negative vertical velocities at the dense side of the front (Figure 6), together with the observed horizontal advection of the isopycnals (Figure 7), can be a result of the ageostrophic

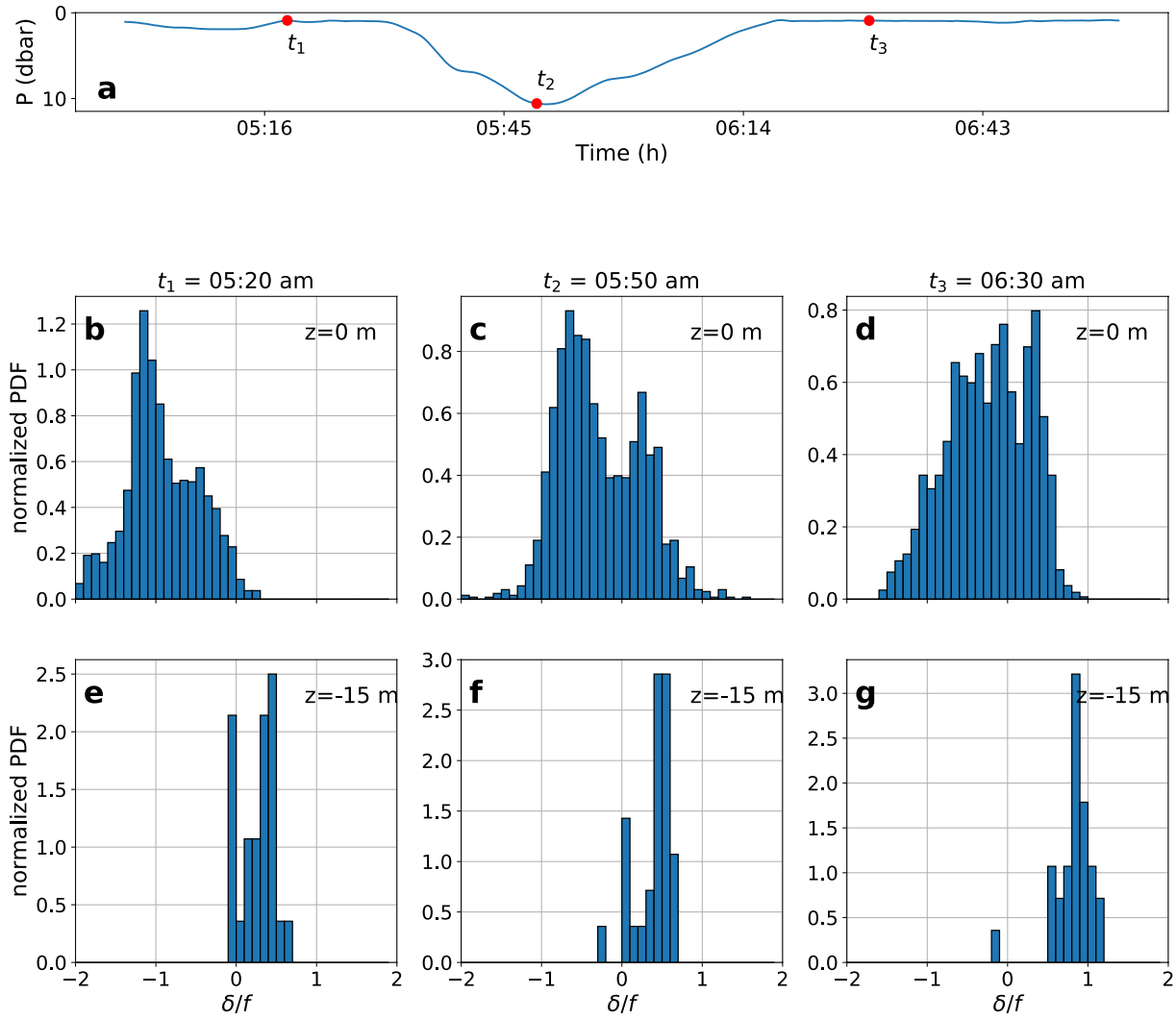

Figure 5. (a) Lagrangian float depth evolution during the subduction event. t_1 corresponds to June 1, 2018 5:20 h, t_2 to June 1, 2018 5:50 h, and t_3 to June 1, 2018 06:30 h. (b–g) Histograms of normalized divergence δ/f calculated at high resolution at three instances: left column t_1, middle column t_2, and right column t_3. Top row is divergence at the surface and bottom row is divergence at 15 m depth.

secondary circulation. The secondary circulation is a mechanism present at the submesoscale surface density fronts which acts to restore the geostrophic balance (Capet et al., 2008; Gula et al., 2015; Sullivan & McWilliams, 2018). An ageostrophic secondary circulation acts as an overturning circulation that counteracts the steepening of isopycnals. It functions as a conduit from the balanced circulation to smaller scales, and eventually to dissipation scales. Multiple dynamical mechanisms have been described that can generate a departure from geostrophic balance leading to an ageostrophic circulation such as turbulent thermal wind balance, Ekman buoyancy fluxes, frontogenesis, mixed-layer instability, and interaction with topography (McWilliams, 2016). Here, frontogenesis of the $\mathcal{O}$(1 m/s) mesoscale flow is likely a dominant mechanism to energize motions at submesocale and smaller scales that can lead to strong ageostrophic circulation.

5.2. Vertical Velocity Estimation

The vertical velocities from the drifter-computed divergence obtained in this study (45 m day^{-1}) are consistent with values reported by previous studies in in the Alboran Sea with other methods (10–50 m day^{-1}) (Allen et al., 2001; Flexas et al., 2006; Oguz et al., 2014; Tintoré et al., 1991). We also studied vertical velocity associated with the strongest convergence and obtained a downward speed of 100 m day^{-1}. This value,

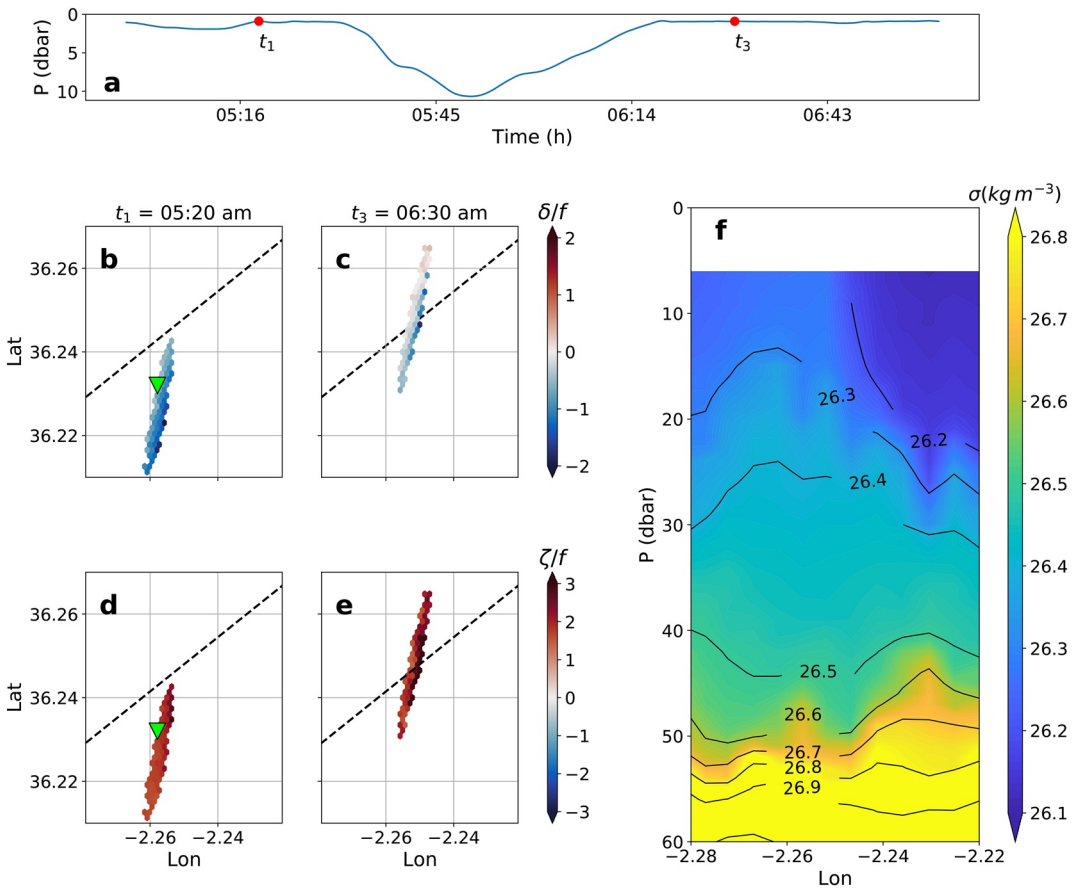

Figure 6. (a) Lagrangian float depth evolution during the subduction event. As in Figure 5, t_1 corresponds to June 1, 2018 5:20 h and t_3 to June 1, 2018 06:30 h. (b–e) Normalized divergence δ/f (top row) and vertical vorticity ζ/f (bottom row) obtained from surface clusters. Left column shows values at t_1 and right column values at t_2. The downward green triangle in panels (b and d) indicates the estimated position of subduction of the float. In each bin, the median value of all data points is plotted, containing at least 10 data points. The black dashed line shows the location of the UCTD section shown in panel (f). (f) Vertical section of potential density anomaly obtained from UCTD data. UCTD, Underway-CTD.

although smaller than the one measured by the float (740 m day^{-1} during the subduction), provides a significantly larger downward speed than those measured previously in the region. Yet, for context, D'Asaro et al. (2018) found vertical velocity of 1,700 m day^{-1} from a Lagrangian float in submesoscale turbulence in the Gulf of Mexico.

The difference between vertical velocities obtained from drifters and the Lagrangian float is expected and can be caused by several factors. First, the drifters may be under-resolving the kinematic properties due to an anisotropic measurement along the gyre. This would be caused, not by the strong mean current, as we remove this component in the LS method, but by the strong. Horizontal shear generated at the edges of the gyre. The shear causes the clusters to elongate quickly in the direction of the mean current, and therefore capture only one component of the horizontal divergence field. Still, this effect should be small at early times thanks to the large number of drifters. Certainly, it will have an impact once all the clusters are elongated by the gyre shear. Second, there is a scale difference between the measurements done by clusters of drifters and by the Lagrangian float. Although we focused on the closest clusters around the float, the float measures much smaller scales. The float observations have a resolution of meters and seconds while the drifters have space-time resolution of hundreds of meters and minutes. Hence, this difference can come from the fact that we are characterizing an intense event of subduction at two different scales or, that the float is actually experiencing a region of strong convergence much smaller than the clusters of drifters can resolve.

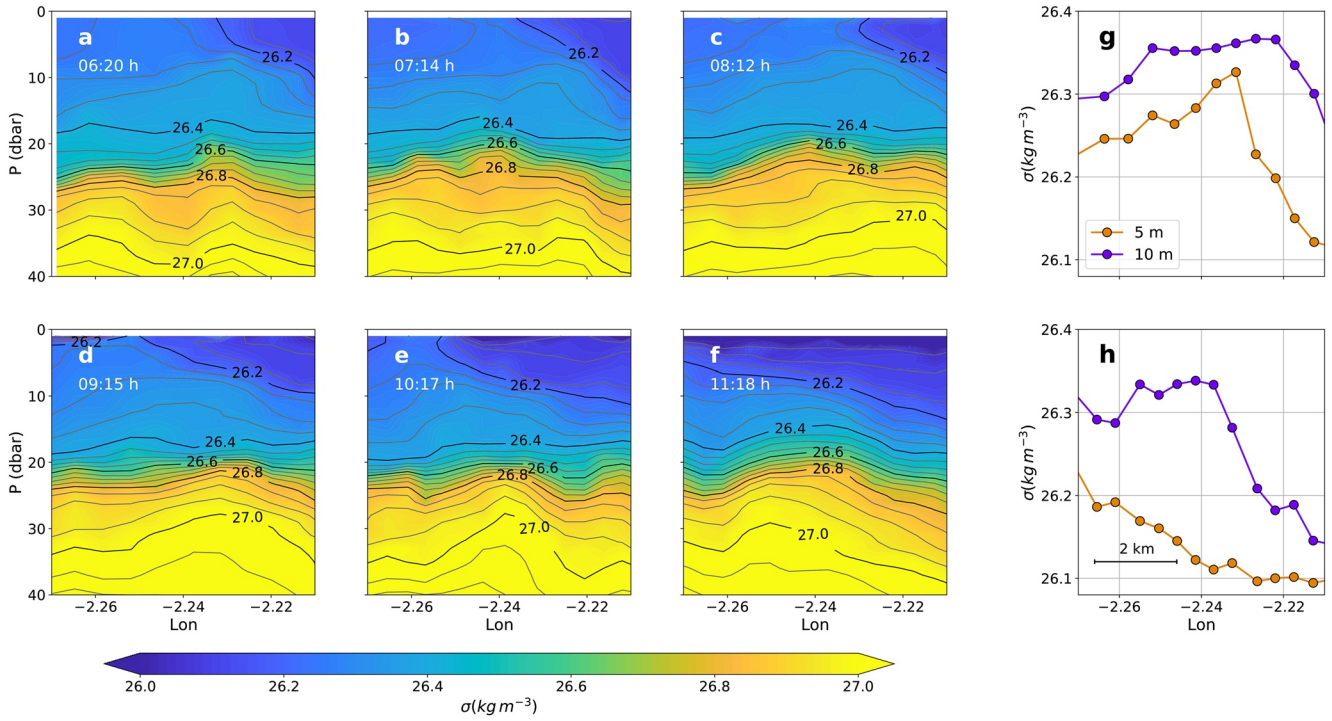

Figure 7. (a–f) Time evolution of a vertical section of potential density anomaly located at 36.3°N. All timestamps correspond to June 1, 2018. (g and h) Horizontal slices through c and f, respectively, showing potential density anomaly at 5-m (orange) and 10-m (purple) line.

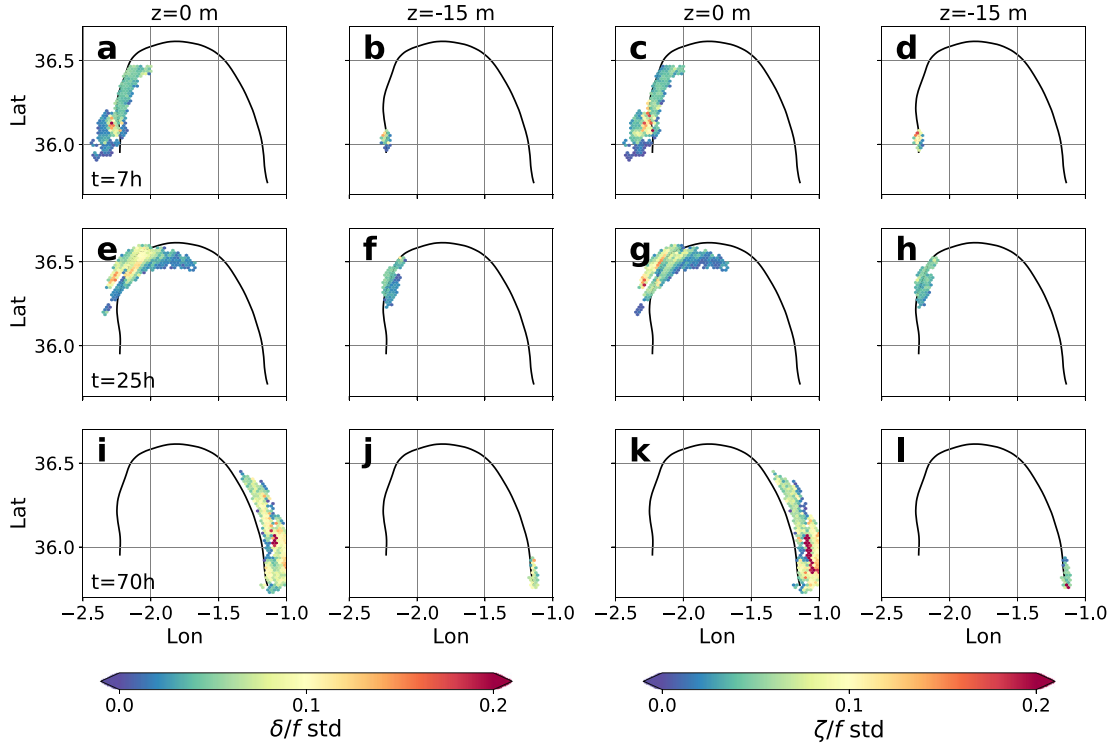

Figure 8. As Figure 3 but each bin value represents the standard deviation of all data points in each bin.

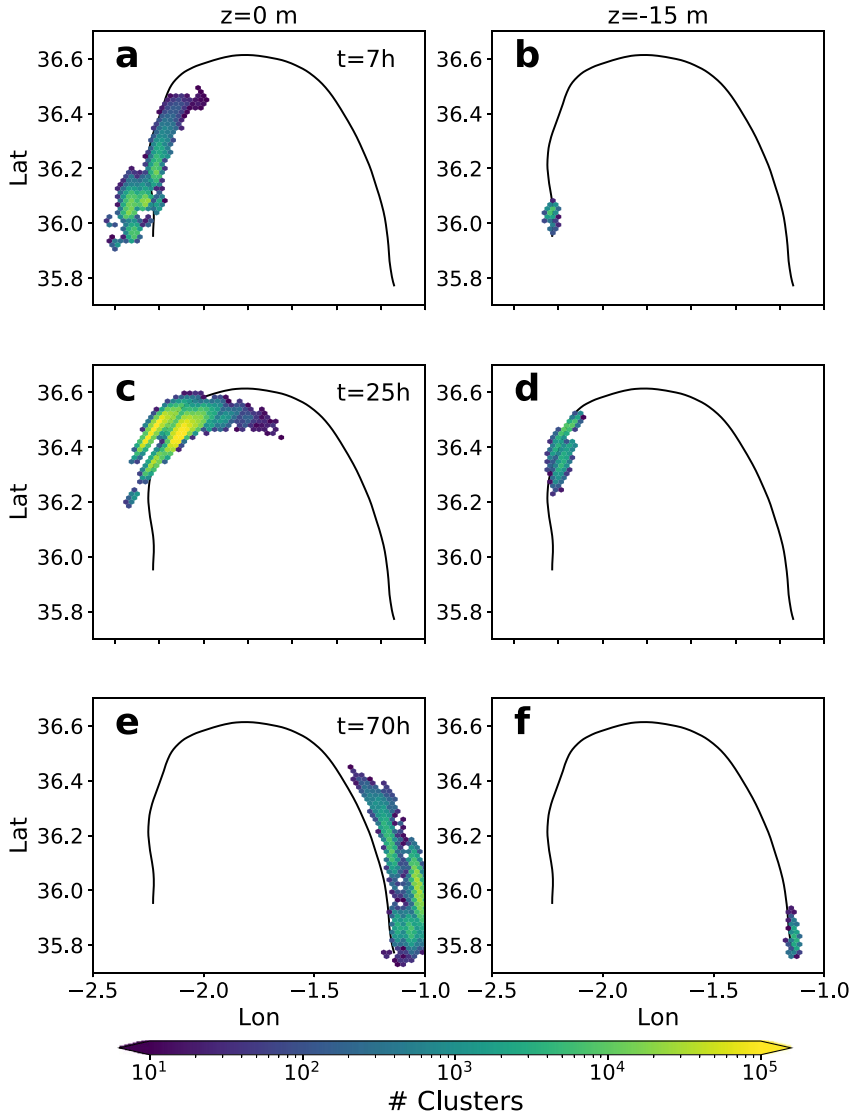

Figure 9. Quantity of clusters per bin in Figures 3 and 8.

5.3. Uncertainties in the Kinematic Properties

Although we selected the optimal parameters for the drifter clusters for the kinematic-property estimation, we expect that our results have uncertainty.

We expect that gradient properties such as vertical vorticity, lateral strain rate, and divergence have a large variability at the underresolved scales (Lien & Müller, 1992; Lien & Sanford, 2019; Müller et al., 1988). Consequently, any polygon that is used to estimate gradient properties at a particular scale will alias the motions at the smallest, unresolved scales. Aliasing is known to fold the variance that would occur at small scales into the larger scales and, therefore, potentially affects the accuracy of the resulting gradient estimation.

Apart from this, the large number of clusters can imply large spread of values if the method is not precise and robust enough. We reproduce Figure 3 by visualizing the standard deviation of all clusters in each bin Figure 8. We obtain values mostly around $0.1f$ for both divergence and vertical vorticity. These values represent the standard deviation for all data points in each bin and have been calculated also for different grid sizes to ensure that they are not gridsize-dependent (not shown). The standard deviations are not a function of the number of clusters per bin either (Figure 9).

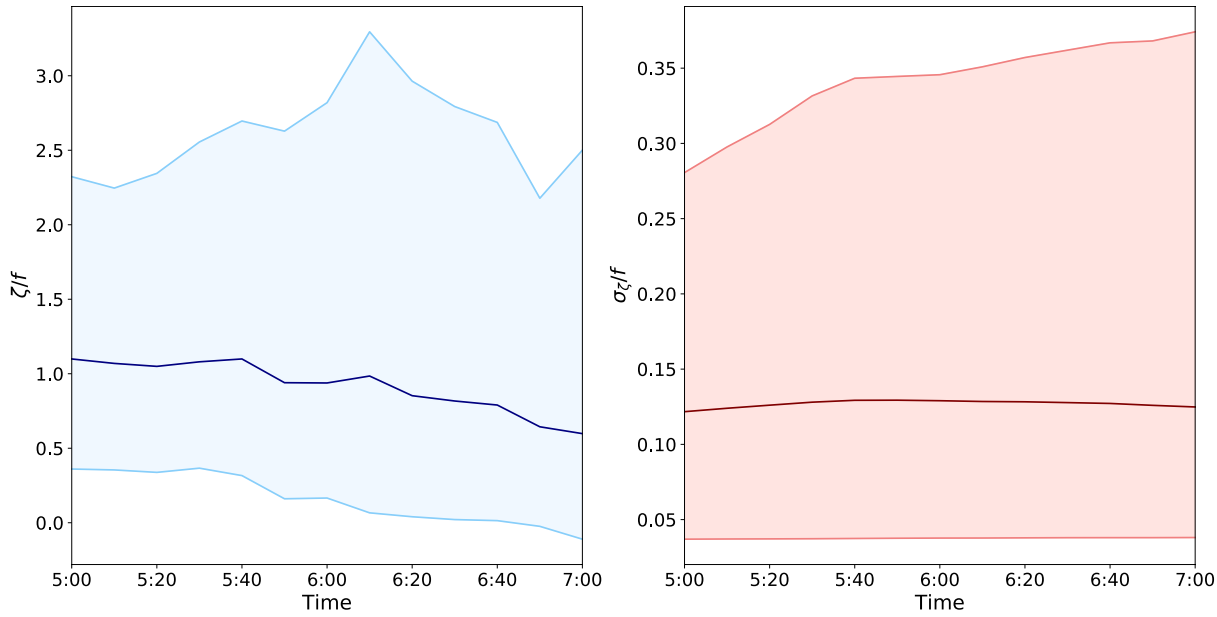

Figure 10. Timeseries during the event of subduction for (a) the normalized vertical vorticity ζ/f and (b) the normalized vorticity variance error σ_ζ/f. At each timestep, the PDF of all available values is used to find the 95% confidence interval. The results shown correspond to the surface clusters.

Acknowledging these potential sources of error, we cross-examine independent measurement platforms to understand the robustness of our findings. First, we use surface and subsurface drifters and analyze the trajectories for both in the same way. Both agree in terms of the qualitative patterns in the vorticity and divergence distributions. Second, we compare the timing, magnitude, and location of drifter-derived convergence with the behavior of a Lagrangian float. As shown in Figures 5 and 6. We then derive vertical velocity smaller but about the same order of magnitude as vertical velocity from the Lagrangian float. Third, the patterns and magnitude of the divergence and vorticity agree with our understanding of a submesoscale meander gained from previous observation, theory, and modeling. Finally, we study the effect of the GPS error on our results, we study the vorticity error variance in the submesoscale estimates. The results shown in Figure 10 indicate an error of up to 10% of the kinematic-property value. If the flow field was not under-resolved by the LS method, this would be the actual error of the results. The effect of the GPS error together with the low variance of the cluster-estimates in each bin (Figure 8), indicate the robustness of the results presented in this work.

6. Conclusions

Clusters of drifters were used to obtain spatial distributions as well as timeseries of vertical vorticity and horizontal divergence at a surface density front in the Alboran Sea. The schemed deployment of 51 drifters with a maximum cross-array length of 12 km allowed us to study both mesoscale and submesoscale length scales. Thanks to the deployment of drifters at two different depths, we were able to evaluate the vertical structure of divergence in the upper 15 m, allowing to estimate vertical velocity. In addition to the drifter analysis, the deployment of a Lagrangian float and UCTD surveys provided a detailed context of the submesoscale dynamics on the west part of the gyre.

Our results with drifter clusters at the mesoscale length scales describe the expected circulation of the gyre. Meanwhile, at the submesoscale length scale, high-resolution observations revealed a high spatiotemporal variability in the divergence and vorticity field. In particular, a strong subduction event was measured simultaneously by clusters of drifters and a Lagrangian float. The subduction of the float was consistent with the patterns of convergence measured from drifters. The high-density variability of the 2-km-wide front also showed up in a repeated section of UCTD casts with subduction occurring where horizontal density gradients were large.

In future experiments, the results of kinematic-property estimation from drifters can be improved in several ways. From a methodology point of view, an increase in GPS accuracy will reduce the error of the velocity gradients calculations, especially for small length scale and short timescale flows. Furthermore, if computational cost is not limiting, the use of a higher number of drifter per experiment and cluster can reduce the residual of the velocity gradient fit. From an experimental point of view, due to the lateral frontal shear, drifters tend to converge in a narrow region in the center of the current. This causes drifter clusters to elongate and spread to larger scales at which they no longer measure the two-dimensional velocity field representatively. Consequently, the number of clusters available for the kinematic properties computation drops significantly just a few hours after the deployment. Repeated deployments of drifter arrays would increase significantly the amount of clusters with optimal length scale and aspect ratio to perform the LS method.

Data Availability Statement

Datasets for this research are available in this in-text data citation reference: Tarry et al. (2021). The altimeter products were produced and distributed by CMEMS (https://marine.copernicus.eu).

Acknowledgments
This research was supported by the Office of Naval Research (ONR) Departmental Research Initiative CALYPSO under program officers Terri Paluszkiewicz and Scott Harper. The authors' ONR grant numbers are as follows: D. R. Tarry, A. Pascual, S. Ruiz and A. Mahadevan N000141613130, S. Essink N000146101612470, P.-M. Poulain N000141812418, T. OÖzgökmen N000141812138, L. R. Centurioni N000141712517 and N00014191269, T. Farrar N000141812431, A. Shcherbina N000141812139 and N000141812420, and E. A. D'Asaro N000141812139. Measurements were conducted from the NRV Alliance. We are grateful to the captain and crew and the technical and scientific staff involved in making measurements. Also special thanks to Matthew Spydell for the useful conversation about the kinematic properties error estimation.

References

Allen, J. T., Painter, S. C., & Rixen, M. (2008). Eddy transport of western Mediterranean intermediate water to the Alboran sea. *Journal of Geophysical Research*, *113*, C04024. https://doi.org/10.1029/2007JC004649

Allen, J. T., Smeed, D. A., Tintoré, J., & Ruiz, S. (2001). Mesoscale subduction at the Almeria-Oran front. *Journal of Marine Systems*, *30*(3), 263–285. https://doi.org/10.1016/S0924-7963(01)00062-8

Alpers, W., Brandt, P., Lazar, A., Dagorne, D., Sow, B., Faye, S., et al. (2013). A small-scale oceanic eddy off the coast of west Africa studied by multi-sensor satellite and surface drifter data. *Remote Sensing of Environment*, *129*, 132–143. https://doi.org/10.1016/j.rse.2012.10.032

Berta, M., Griffa, A., Haza, A. C., Horstmann, J., Huntley, H. S., Ibrahim, R., et al. (2020). Submesoscale kinematic properties in summer and winter surface flows in the northern gulf of Mexico. *Journal of Geophysical Research: Oceans*, *125*, e2020JC016085. https://doi.org/10.1029/2020JC016085

Berta, M., Griffa, A., Özgökmen, T. M., & Poje, A. C. (2016). Submesoscale evolution of surface drifter triads in the Gulf of Mexico. *Geophysical Research Letters*, *43*, 11751–11759. https://doi.org/10.1002/2016GL070357

Capet, X., McWilliams, J. C., Molemaker, M. J., & Shchepetkin, A. F. (2008). Mesoscale to submesoscale transition in the California current system. Part I: Flow structure, eddy flux, and observational tests. *Journal of Physical Oceanography*, *38*(1), 29–43. https://doi.org/10.1175/2007JPO3671.1

Charney, J. G. (1971). Geostrophic turbulence. *Journal of the Atmospheric Sciences*, *28*(6), 1087–1095. https://doi.org/10.1175/1520-0469(1971)028<1087:GT>2.0.CO;2

Choi, J., Bracco, A., Barkan, R., Shchepetkin, A. F., McWilliams, J. C., & Molemaker, J. M. (2017). Submesoscale dynamics in the Northern Gulf of Mexico. Part III: Lagrangian implications. *Journal of Physical Oceanography*, *47*(9), 2361–2376. https://doi.org/10.1175/jpo-d-17-0036.1

Cotroneo, Y., Aulicino, G., Ruiz, S., Pascual, A., Budillon, G., Fusco, G., & Tintoré, J. (2016). Glider and satellite high resolution monitoring of a mesoscale eddy in the Algerian basin: Effects on the mixed layer depth and biochemistry. *Journal of Marine Systems*, *162*, 73–88. https://doi.org/10.1016/j.jmarsys.2015.12.004

D'Asaro, E. A. (2003). Performance of autonomous Lagrangian floats. *Journal of Atmospheric and Oceanic Technology*, *20*(6), 896–911. https://doi.org/10.1175/1520-0426(2003)020⟨0896:POALF⟩2.0.CO;2

D'Asaro, E. A., Shcherbina, A. Y., Klymak, J. M., Molemaker, J., Novelli, G., Guigand, C. M., et al. (2018). Ocean convergence and the dispersion of flotsam. *Proceedings of the National Academy of Sciences of the United States of America*, *115*(6), 1162–1167. https://doi.org/10.1073/pnas.1718453115

Davis, R. E. (1985). Drifter observations of coastal surface currents during code: The method and descriptive view. *Journal of Geophysical Research*, *90*(C3), 4741–4755. https://doi.org/10.1029/JC090iC03p04741

Dever, M., Freilich, M., Hodges, B., Farrar, T., Lanagan, T., & Mahadevan, A. (2019). *UCTD and ECOCTD observations from the calypso pilot experiment (2018): Cruise and data report (Tech. Rep. WHOI-2019-01)*. Falmouth, MA: Woods Hole Oceanographic Institution. https://doi.org/10.1575/1912/23637

Ducet, N., Le Traon, P. Y., & Reverdin, G. (2000). Global high-resolution mapping of ocean circulation from TOPEX/Poseidon and ERS-1 and -2. *Journal of Geophysical Research*, *105*(C8), 19477–19498. https://doi.org/10.1029/2000JC900063

Escudier, R., Renault, L., Pascual, A., Brasseur, P., Chelton, D., & Beuvier, J. (2016). Eddy properties in the western Mediterranean sea from satellite altimetry and a numerical simulation. *Journal of Geophysical Research: Oceans*, *121*(6), 3990–4006. https://doi.org/10.1002/2015JC011371

Estrada-Allis, S. N., Barceló-Llull, B., Pallàs-Sanz, E., Rodríguez-Santana, A., Souza, J. M. A. C., Mason, E., et al. (2019). Vertical velocity dynamics and mixing in an anticyclone near the Canary Islands. *Journal of Physical Oceanography*, *49*(2), 431–451. https://doi.org/10.1175/JPO-D-17-0156.1

Flexas, M. M., Gomis, D., Ruiz, S., Pascual, A., & León, P. (2006). In situ and satellite observations of the eastward migration of the western Alboran sea gyre. *Progress in Oceanography*, *70*(2), 486–509. https://doi.org/10.1016/j.pocean.2006.03.017

Freilich, M. A., & Mahadevan, A. (2019). Decomposition of vertical velocity for nutrient transport in the upper ocean. *Journal of Physical Oceanography*, *49*(6), 1561–1575. https://doi.org/10.1175/jpo-d-19-0002.1

Gomis, D., Ruiz, S., & Pedder, M. A. (2001). Diagnostic analysis of the 3d ageostrophic circulation from a multivariate spatial interpolation of CTD and ADCP data. *Deep Sea Research I: Oceanographic Research Papers*, *48*(1), 269–295. https://doi.org/10.1016/S0967-0637(00)00060-1

Gula, J., Molemaker, M. J., & McWilliams, J. C. (2015). Gulf stream dynamics along the Southeastern U.S. seaboard. *Journal of Physical Oceanography*, *45*(3), 690–715. https://doi.org/10.1175/JPO-D-14-0154.1

Haza, A. C., Özgökmen, T. M., & Hogan, P. (2016). Impact of submesoscales on surface material distribution in a gulf of Mexico mesoscale eddy. *Ocean Modelling*, *107*, 28–47. https://doi.org/10.1016/j.ocemod.2016.10.002

Houpert, L., Testor, P., Durrieu de Madron, X., Somot, S., D'Ortenzio, F., Estournel, C., & Lavigne, H. (2015). Seasonal cycle of the mixed layer, the seasonal thermocline and the upper-ocean heat storage rate in the Mediterranean sea derived from observations. *Progress in Oceanography*, *132*, 333–352. https://doi.org/10.1016/j.pocean.2014.11.004

Kawai, H. (1985). Scale dependence of divergence and vorticity of near-surface flows in the sea. *Journal of the Oceanographical Society of Japan*, *41*(3), 157–166. https://doi.org/10.1007/bf02111115

LaCasce, J. H. (2008). Lagrangian Statistics from oceanic and atmospheric observations (Vol. 744, pp. 165–218), Berlin:Springer.

Lévy, M., Klein, P., & Treguier, A.-M. (2001). Impact of sub-mesoscale physics on production and subduction of phytoplankton in an oligotrophic regime. *Journal of Marine Research*, *59*(4), 535–565. https://doi.org/10.1357/002224001762842181

Lien, R.-C., & Müller, P. (1992). Normal-mode decomposition of small-scale oceanic motions. *Journal of Physical Oceanography*, *22*(12), 1583–1595. https://doi.org/10.1175/1520-0485(1992)022<1583:NMDOSS>2.0.CO;2

Lien, R.-C., & Sanford, T. B. (2019). Small-scale potential vorticity in the upper-ocean thermocline. *Journal of Physical Oceanography*, *49*, 1845. https://doi.org/10.1175/jpo-d-18-0052.1

Mahadevan, A., & Archer, D. (2000). Modeling the impact of fronts and mesoscale circulation on the nutrient supply and biogeochemistry of the upper ocean. *Journal of Geophysical Research*, *105*(C1), 1209–1225. https://doi.org/10.1029/1999JC900216

Mahadevan, A., Pascual, A., Rudnick, D. L., Ruiz, S., Tintoré, J., & D'Asaro, E. (2020). Coherent pathways for vertical transport from the surface ocean to interior. *Bulletin of the American Meteorological Society*, *101*, E1996. https://doi.org/10.1175/BAMS-D-19-0305.1

Mahadevan, A., Spiro Jaeger, G., Freilich, M., Omand, M., Shroyer, E., & Sengupta, D. (2016). Freshwater in the Bay of Bengal: Its fate and role in air-sea heat exchange. *Oceanography*, *29*(2), 72–81. https://doi.org/10.5670/oceanog.2016.40

Mahadevan, A., & Tandon, A. (2006). An analysis of mechanisms for submesoscale vertical motion at ocean fronts. *Ocean Modelling*, *14*(3), 241–256. https://doi.org/10.1016/j.ocemod.2006.05.006

Mason, E., Ruiz, S., Bourdalle-Badie, R., Reffray, G., García-Sotillo, M., & Pascual, A. (2019). New insight into 3-d mesoscale eddy properties from CMEMS operational models in the western Mediterranean. *Ocean Science*, *15*(4), 1111–1131. https://doi.org/10.5194/os-15-1111-2019

Mauri, E., & Poulain, P. (2004). *Wind-driven currents in Mediterranean drifter-data* (OGS Tech. Rep. 01/2004/OGA/1).

McWilliams, J. C. (2016). Submesoscale currents in the ocean. *Proceedings of the Royal Society A*, *472*(2189), 20160117. https://doi.org/10.1098/rspa.2016.0117

McWilliams, J. C., Gula, J., & Molemaker, M. J. (2019). The gulf stream north wall: Ageostrophic circulation and frontogenesis. *Journal of Physical Oceanography*, *49*(4), 893–916. https://doi.org/10.1175/JPO-D-18-0203.1

Molinari, R., & Kirwan, A. D. (1975). Calculations of differential kinematic properties from Lagrangian observations in the Western Caribbean Sea. *Journal of Physical Oceanography*, *5*(3), 483–491. https://doi.org/10.1175/1520-0485(1975)005(0483:CODKPF)2.0.CO;2

Müller, P., Lien, R.-C., & Williams, R. (1988). Estimates of potential vorticity at small scales in the ocean. *Journal of Physical Oceanography*, *18*(3), 401–416. https://doi.org/10.1175/1520-0485(1988)018<0401:EOPVAS>2.0.CO;2

Niiler, P. P., Sybrandy, A. S., Bi, K., Poulain, P. M., & Bitterman, D. (1995). Measurements of the water-following capability of holey-sock and TRISTAR drifters. *Deep Sea Research Part I: Oceanographic Research Papers*, *42*(11–12), 1951–1964. https://doi.org/10.1016/0967-0637(95)00076-3

Niller, P. P., Poulain, P.-M., & Haury, L. R. (1989). Synoptic three-dimensional circulation in an onshore-flowing filament of the California Current. *Deep Sea Research A: Oceanographic Research Papers*, *36*(3), 385–405. https://doi.org/10.1016/0198-0149(89)90043-5

Novelli, G., Guigand, C. M., Cousin, C., Ryan, E. H., Laxague, N. J. M., Dai, H., et al. (2017). A biodegradable surface drifter for ocean sampling on a massive scale. *Journal of Atmospheric and Oceanic Technology*, *34*(11), 2509–2532. https://doi.org/10.1175/JTECH-D-17-0055.1

Oguz, T., Macias, D., Garcia-Lafuente, J., Pascual, A., & Tintore, J. (2014). Fueling plankton production by a meandering frontal jet: A case study for the Alboran sea (western Mediterranean). *PloS One*, *9*(11), e111482. https://doi.org/10.1371/journal.pone.0111482

Ohlmann, J. C., Molemaker, M. J., Baschek, B., Holt, B., Marmorino, G., & Smith, G. (2017). Drifter observations of submesoscale flow kinematics in the coastal ocean. *Geophysical Research Letters*, *44*(1), 330–337. https://doi.org/10.1002/2016GL071537

Okubo, A., & Ebbesmeyer, C. C. (1976). Determination of vorticity, divergence, and deformation rates from analysis of drogue observations. *Deep Sea Research and Oceanographic Abstracts*, *23*(4), 349–352. https://doi.org/10.1016/0011-7471(76)90875-5

Omand, M. M., D'Asaro, E. A., Lee, C. M., Perry, M. J., Briggs, N., Cetini , I., & Mahadevan, A. (2015). Eddy-driven subduction exports particulate organic carbon from the spring bloom. *Science*, *348*(6231), 222–225. https://doi.org/10.1126/science.1260062

Paduan, J. D., & Niiler, P. P. (1990). A Lagrangian description of motion in Northern California coastal transition filaments. *Journal of Geophysical Research*, *95*(C10), 18095–18109. https://doi.org/10.1029/jc095ic10p18095

Pallàs-Sanz, E., Johnston, T. M. S., & Rudnick, D. L. (2010). Frontal dynamics in a california current system shallow front. 2: Mesoscale vertical velocity. *Journal of Geophysical Research*, *115*, C12068. https://doi.org/10.1029/2010JC006474

Pascual, A., Gomis, D., Haney, R. L., & Ruiz, S. (2004). A quasigeostrophic analysis of a meander in the Palamós canyon: Vertical velocity, geopotential tendency, and a relocation technique. *Journal of Physical Oceanography*, *34*(10), 2274–2287.

Pascual, A., Ruiz, S., Olita, A., Troupin, C., Claret, M., Casas, B., et al. (2017). A multiplatform experiment to unravel meso- and submesoscale processes in an intense front (Alborex). *Frontiers in Marine Science*, *4*, 39. https://doi.org/10.3389/fmars.2017.00039

Poulain, P.-M., Bussani, A., Gerin, R., Jungwirth, R., Mauri, E., Menna, M., & Notarstefano, G. (2013). Mediterranean surface currents measured with drifters: From basin to subinertial scales. *Oceanography*, *26*(1), 38–47

Poulain, P.-M., & Gerin, R. (2019). Assessment of the water-following capabilities of code drifters based on direct relative flow measurements. *Journal of Atmospheric and Oceanic Technology*, *36*(4), 621–633. https://doi.org/10.1175/JTECH-D-18-0097.1

Poulain, P.-M., Gerin, R., Mauri, E., & Pennel, R. (2009). Wind effects on drogued and undrogued drifters in the eastern Mediterranean. *Journal of Atmospheric and Oceanic Technology*, *26*(6), 1144–1156. https://doi.org/10.1175/2008JTECHO618.1

Renault, L., Oguz, T., Pascual, A., Vizoso, G., & Tintore, J. (2012). Surface circulation in the Alborán Sea (western Mediterranean) inferred from remotely sensed data. *Journal of Geophysical Research*, *117*, C08009. https://doi.org/10.1029/2011JC007659

Rio, M.-H., & Hernandez, F. (2003). High-frequency response of wind-driven currents measured by drifting buoys and altimetry over the world ocean. *Journal of Geophysical Research*, *108*(C8), 3283. https://doi.org/10.1029/2002JC001655

Rudnick, D. L., & Klinke, J. (2007). The underway conductivity-temperature-depth instrument. *Journal of Atmospheric and Oceanic Technology*, *24*(11), 1910–1923. https://doi.org/10.1175/JTECH2100.1

Ruiz, S., Claret, M., Pascual, A., Olita, A., Troupin, C., Capet, A., et al. (2019). Effects of oceanic mesoscale and submesoscale frontal processes on the vertical transport of phytoplankton. *Journal of Geophysical Research: Oceans*, *124*, 5999–6014. https://doi.org/10.1029/2019JC015034

Ruiz, S., Pascual, A., Garau, B., Pujol, I., & Tintoré, J. (2009). Vertical motion in the upper ocean from glider and altimetry data. *Geophysical Research Letters*, *36*, L14607. https://doi.org/10.1029/2009GL038569

Saucier, W. J. (1955). *Principles of meteorological analysis*.Chicago, IL: University of Chicago Press.

Shcherbina, A. Y., D'Asaro, E. A., & Nylund, S. (2018). Observing finescale oceanic velocity structure with an autonomous Nortek acoustic doppler current profiler. *Journal of Atmospheric and Oceanic Technology*, *35*(2), 411–427. https://doi.org/10.1175/JTECH-D-17-0108.1

Siegelman, L., Klein, P., Rivière, P., Thompson, A. F., Torres, H. S., Flexas, M., & Menemenlis, D. (2020). Enhanced upward heat transport at deep submesoscale ocean fronts. *Nature Geoscience*, *13*(1), 50–55. https://doi.org/10.1038/s41561-019-0489-1

Sotillo, M. G., García-Ladona, E., Orfila, A., Rodríguez-Rubio, P., Maraver, J. C., Conti, D., et al. (2016). The medess-gib database: Tracking the Atlantic water inflow. *Earth System Science Data*, *8*, 141–149. https://doi.org/10.5194/essd-8-141-2016

Spydell, M. S., Feddersen, F., & Macmahan, J. (2019). The effect of drifter GPS errors on estimates of submesoscale vorticity. *Journal of Atmospheric and Oceanic Technology*, *36*(11), 2101–2119. https://doi.org/10.1175/JTECH-D-19-0108.1

Sullivan, P. P., & McWilliams, J. C. (2018). Frontogenesis and frontal arrest of a dense filament in the oceanic surface boundary layer. *Journal of Fluid Mechanics*, *837*, 341–380. https://doi.org/10.1017/jfm.2017.833

Swenson, M. S., Niiler, P. P., Brink, K. H., & Abbott, M. R. (1992). Drifter observations of a cold filament off Point Arena, California, in July 1988. *Journal of Geophysical Research*, *97*(C3), 3593–3610. https://doi.org/10.1029/91JC02736

Sybrandy, A. L., & Niiler, P. P. (1991). The WOCE/TOGASVP Lagrangian drifter construction manual (*WOCE Rep*. *63*, pp. 58). Retrieved from https://ci.nii.ac.jp/naid/10004496389/en/

Tarry, D. R., Essink, S., Pascual, A., Ruiz, S., Poulain, P. M., Özgökmen, T., et al. (2021). *Dataset to accompany "Frontal Convergence and Vertical Velocity measured by Drifters in the Alboran Sea"*. Zenodo. https://doi.org/10.5281/zenodo.4592311

Tintoré, J., Gomis, D., Alonso, S., & Parrilla, G. (1991). Mesoscale Dynamics and Vertical Motion in the Alborán Sea. *Journal of Physical Oceanography*, *21*(6), 811–823. https://doi.org/10.1175/1520-0485(1991)021<0811:MDAVMI>2.0.CO;2

Tintoré, J., Gomis, D., Alonso, S., & Wang, D.-P. (1988). A theoretical study of large sea level oscillations in the western Mediterranean. *Journal of Geophysical Research*, *93*(C9), 10797–10803. https://doi.org/10.1029/JC093iC09p10797

Traon, P. Y. L., Nadal, F., & Ducet, N. (1998). An improved mapping method of multisatellite altimeter data. *Journal of Atmospheric and Oceanic Technology*, *15*(2), 522–534. https://doi.org/10.1175/1520-0426(1998)015⟨0522:AIMMOM⟩2.0.CO;2

Yu, X., Naveira Garabato, A. C., Martin, A. P., Buckingham, C. E., Brannigan, L., & Su, Z. (2019). An annual cycle of submesoscale vertical flow and restratification in the upper ocean. *Journal of Physical Oceanography*, *49*(6), 1439–1461. https://doi.org/10.1175/JPO-D-18-0253.1